

IEEE 802.11bf Multistatic Sensing with Unsynchronized Receivers

Abdallah, Ayah; Zhou, Shengli; Wang, Pu

TR2025-080 June 10, 2025

Abstract

Distinct from existing works on millimeter wave Wi-Fi sensing in a monostatic or bistatic setting, in this paper we present a complete framework for multistatic sensing with unsynchronized receivers using IEEE 802.11bf signals. Based on the channel estimates from the active sensing procedure, each receiver extracts the line-of-sight and the target-reflected paths, and reports the time-difference-of-arrivals to a central server, which localizes and potentially tracks the target. We simulate the system using the QD channel simulator and the ISAC-PLM software package from NIST, and present the measurement accuracy at each receiver and the localization accuracy at the central server. Numerical results show promising localization performance at reasonable signal-to-noise ratio (SNR) levels.

IEEE Statistical Signal Processing Workshop (SSP) 2025

IEEE 802.11bf Multistatic Sensing with Unsynchronized Receivers

Ayah Abdallah[†], Shengli Zhou[†], Pu (Perry) Wang[‡]

[†]Department of Electrical and Computer Engineering, University of Connecticut, Storrs, CT 06250, USA

[‡]Mitsubishi Electric Research Laboratories (MERL), Cambridge, MA 02139, USA

Abstract—Distinct from existing works on millimeter wave Wi-Fi sensing in a monostatic or bistatic setting, in this paper we present a complete framework for multistatic sensing with unsynchronized receivers using IEEE 802.11bf signals. Based on the channel estimates from the active sensing procedure, each receiver extracts the line-of-sight and the target-reflected paths, and reports the time-difference-of-arrivals to a central server, which localizes and potentially tracks the target. We simulate the system using the QD channel simulator and the ISAC-PLM software package from NIST, and present the measurement accuracy at each receiver and the localization accuracy at the central server. Numerical results show promising localization performance at reasonable signal-to-noise ratio (SNR) levels.

Index Terms—Wi-Fi, IEEE 802.11bf, active sensing, multistatic, NIST, ISAC-PLM, QD channel simulator

I. INTRODUCTION

With the massive deployment of Wi-Fi devices and anticipated market growth, enabling sensing functionalities to future Wi-Fi technologies has attracted interest from academia and industry. Wi-Fi sensing can be categorized into sub-7-GHz Wi-Fi sensing [1] and directional multi-gigabit (DMG) Wi-Fi sensing at frequencies above 45 GHz [2]–[5]. As a unique feature of IEEE 802.11ad/ay, DMG beam training is usually initiated by the access point (AP) during the beacon transmission interval (BTI), where directional frames are transmitted over sector-level beampatterns to probe the environment. In addition to DMG passive sensing, IEEE 802.11bf standard introduces an active sensing procedure defined along the beam refinement protocol (BRP) inserted at the end of data transmission [5].

There are a large body of recent works of DMG sensing in [6]–[11] for outdoor automotive applications and in [12]–[15] for indoor monitoring applications. This paper studies indoor sensing with IEEE 802.11bf signals, which can find applications in smart factories, smart hospitals, and smart homes. This work has the following distinctions. First, existing works adopt either a monostatic setting where a full-duplex operation at the co-located transmitter and receiver [6]–[14], or a bi-static setting with one transmitter and one receiver [15]. This work considers a multistatic setting with one active transmitter and multiple unsynchronized receivers. Second, this work focuses on active sensing with the BRP procedure, while [6]–[13], [15] have focused on the dual use of the preamble in the beacon transmission or the data transmission.

The contributions of the work are as follows. *First*, we develop the procedure of multistatic sensing with unsynchronized receivers. For each packet, each receiver retrieves the

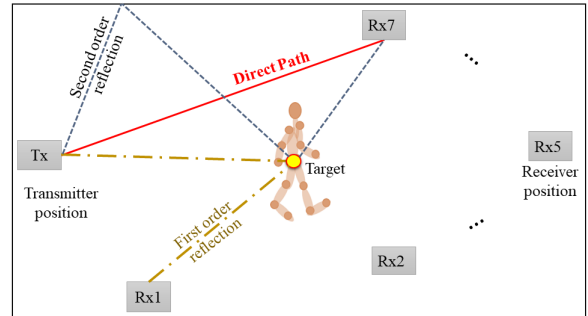


Fig. 1. The indoor system with one transmitter and multiple unsynchronized receivers (7 receivers used in simulation study).

channel state information (CSI) corresponding to different beams. Within a coherent processing interval, the receiver performs two signal processing tasks: (1) identifying the line-of-sight (LoS) path between the transmitter and the receiver, and (2) identifying the reflected path from the target. The time difference of the LoS path and the target path is evaluated and reported to a central server for the localization and tracking of the target. *Second*, we carry out a simulation study based on the Quasi-Deterministic (QD) channel realization software [16] and the “Integrated Sensing and Communication Physical Layer Model (ISAC-PLM)” package [17], developed by the National Institute of Standards and Technology (NIST). We evaluate the measurement accuracy at each receiver and the localization accuracy at the central server. Numerical results show that satisfactory localization performance can be achieved at reasonable signal to noise ratio (SNR) levels. *Third*, our findings highlight the challenges of the proposed approach for practical applications, where receiver placement and dynamic receiver selection will play significant roles in meeting the accuracy requirements.

The rest of this paper is organized as follows. Section II describes the multistatic sensing system setup. Section III addresses the extraction of measurements at each receiver. Section IV presents the localization algorithm at a central server. Section V contains simulation results, and finally Section VI provides a summary of the findings and outlines future research directions.

II. SYSTEM SETUP FOR MULTISTATIC SENSING

The system is illustrated in Fig. 1, with one transmitter, one moving target, and multiple receiver nodes. The receivers

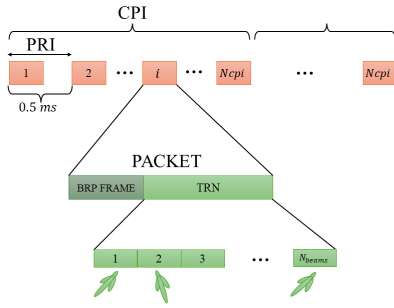


Fig. 2. Defining packet configuration

are positioned at different locations within the room. The monitored target is a point target that resembles the human spine. There are different types of reflected signals from transmitter to the target and the receiver, as follows:

- **Direct path:** the signal along the line-of-sight (LoS) path from the transmitter to a receiver.
- **Reflection paths from environment:** the reflected signals from the transmitter to a receiver after bouncing off the walls, the ground, or the ceiling.
- **First order reflection from target:** the reflected signal to a receiver after it bounces off the target.
- **Second order reflection from target:** the signals that are reflected off both the target and the environment before arriving at the receiver.

The signals along the direct path and the first order reflection off the target provide valuable information for sensing.

Active sensing involves transmitting dedicated sensing packets containing pilot sequences to perform sensing tasks. The IEEE 802.11bf beam refinement protocol (BRP) packets incorporate training (TRN) fields comprising TRN sequences, typically consisting of complementary Golay sequences. These TRNs may be utilized to conduct rapid angular scans covering various directions [5]. The TRN fields consist of multiple units, with each unit containing the direction of a different beamforming configuration, as defined in a codebook [17].

As shown in Fig. 2, there is one packet transmitted for every pulse repetition interval (PRI). Within each TRN segment, there are N_{beams} beamforming directions. The receivers will extract the channel estimates corresponding to each beam direction of each packet and offer measurements useful for localization.

III. EXTRACTING MEASUREMENTS AT EACH RECEIVER

At the i -th packet, there are N_{beams} beamforming configurations. Assume that there are L taps in the discrete-time baseband channel. The baseband samples at each receiver corresponding to the b th beam of the i th packet is

$$y[n; i, b] = \sum_{l=0}^{L-1} h_l[i, b]x[n-l] + w[n; i, b], \quad (1)$$

where $x[n]$ is the known Golay sequence of length 128 in the TRN subfield, $\{h_l[i, b]\}_{l=0}^L$ are the channel taps of the

baseband channel, and $w[n; i, b]$ is additive white Gaussian noise. The complex gain of each tap is estimated via the cross-correlation method as

$$\hat{h}_l[i, b] = \sum_{n=0}^{127} x^*[n]y[n+l; i, b], \quad (2)$$

where $(\cdot)^*$ stands for conjugate. Now collect the estimated channel coefficients into a vector as

$$\mathbf{h}[i, b] = [\hat{h}_1[i, b], \dots, \hat{h}_L[i, b]]^T. \quad (3)$$

For each packet, we will have N_{beams} channel vectors as

$$\{\mathbf{h}[i, b]\}, b = 1, \dots, N_{\text{beams}}. \quad (4)$$

In the numerical study, there are $L = 65$ channel taps and $N_{\text{beams}} = 25$ beams derived from each packet reception.

To present a simple processing framework, we assume that within the coherence processing interval (CPI), the background channels stay static. Each CPI has N_{cpi} packets. We next present the methods used to extract the LoS path and the target path.

A. Direct Path Detection

Define the CIR averaged over the packets within one CPI on each beam as

$$\bar{\mathbf{h}}[b] = \frac{1}{N_{\text{cpi}}} \sum_{i=1}^{N_{\text{cpi}}} \mathbf{h}[i, b]. \quad (5)$$

The LoS path is identified through

$$\hat{l}_{\text{los}} = \arg \max_l \sum_{b=1}^{N_{\text{beams}}} |\bar{h}_l[b]|^2. \quad (6)$$

This method is based on the assumption that the LOS path is the strongest path, if averaged over all beam directions.

B. Target Path Detection

The first step is to remove the “clutter” that contains all the static background of the channel, and then find the peak of the remaining paths. Usually the target response is orders of magnitude weaker than the clutter and so can be hard to detect.

1) *Clutter Removal:* Let us view the average of the channel as the clutter. The channel estimates after removing the static paths are

$$\tilde{\mathbf{h}}[i, b] = \mathbf{h}[i, b] - \bar{\mathbf{h}}[b]. \quad (7)$$

2) *Finding the peak:* The ISAC-PLM software has provided algorithms to find the target path. Along with its principle, we present a simplified processing algorithm for the study in this paper. Corresponding to each tap l and each beam b , we define a vector that contains the tap values from N_{cpi} packets as

$$[\tilde{h}_l[1, b], \dots, \tilde{h}_l[N_{\text{cpi}}, b]]^T. \quad (8)$$

The time variation can be evaluated on a grid of Doppler frequencies with step size Δ_f :

$$\xi_l[b, m] = \sum_{i=1}^{N_{\text{cpi}}} \tilde{h}_l[i, b] e^{-j2\pi i m \Delta_f}. \quad (9)$$

The operation in (9) can be done via zero padding the vector in (8) to length N_{fft} and applying the Fourier transform. A FFT of size 64 is used in this study with $N_{\text{cpi}} = 32$.

Summarizing the information from all the beams, the receiver identifies the target path as:

$$(\hat{l}_{\text{tgt}}, \hat{m}) = \arg \max_{l, m} \sum_{b=1}^{N_{\text{beams}}} |\xi_l[b, m]|^2. \quad (10)$$

C. The Measurement

The time difference between the direct and target paths is $\Delta_\tau = (\hat{l}_{\text{tgt}} - \hat{l}_{\text{los}})/f_s$, where f_s is the sampling rate. The time measurement is converted to a range estimate in meters as

$$z = c\Delta_\tau, \quad (11)$$

where c is the speed of light. The Doppler estimates $\hat{m}\Delta_f$ could be useful when a tracking algorithm is used, which is not pursued in this study.

IV. LOCALIZATION AT CENTRAL SERVER

The measurements from all the receivers will be collected by a central server to carry out the localization task. Let us focus on the localization task within one CPI.

Let z_u denote the estimate from the u th receiver. Set the locations of the transmitter and the u th receiver at:

$$\mathbf{p}_{\text{tx}} = [x_{\text{tx}}, y_{\text{tx}}, z_{\text{tx}}]^T, \quad \mathbf{p}_{\text{rx}, u} = [x_{\text{rx}, u}, y_{\text{rx}, u}, z_{\text{rx}, u}]^T. \quad (12)$$

Assume that the target at the current CPI is at

$$\boldsymbol{\theta} = [\theta_x, \theta_y, \theta_z]^T. \quad (13)$$

The range measurements can be expressed by:

$$z_u = \|\mathbf{p}_{\text{tx}} - \boldsymbol{\theta}\| + \|\boldsymbol{\theta} - \mathbf{p}_{\text{rx}, u}\| - \|\mathbf{p}_{\text{tx}} - \mathbf{p}_{\text{rx}, u}\| + w_u. \quad (14)$$

Note that the noise might not be Gaussian distributed. A grid search is carried out to calculate the target position as

$$\hat{\boldsymbol{\theta}} = \arg \min_{\boldsymbol{\theta}} \sum_{u=1}^{N_r} (z_u - (\|\mathbf{p}_{\text{tx}} - \boldsymbol{\theta}\| + \|\boldsymbol{\theta} - \mathbf{p}_{\text{rx}, u}\| - \|\mathbf{p}_{\text{tx}} - \mathbf{p}_{\text{rx}, u}\|))^2, \quad (15)$$

where N_r is the number of receivers. There would be one position estimate at each CPI. The position estimates across multiple CPIs will form a track of the target.

TABLE I
NODE POSITIONS

	position in $[x, y, z]$
Tx	[3, 0, 2.8]
Rx1	[-3.9, 0, 2.8]
Rx2	[0, -3.4, 2.8]
Rx3	[0, 3.4, 2.8]
Rx4	[3, -3, 2.8]
Rx5	[3, 3.4, 2.8]
Rx6	[0, 0, 3]
Rx7	[0, 3, 2.9]

TABLE II
PHYSICAL PARAMETERS

Parameters	Values
f_s	1.75 GHz
f_c	60 GHz
Training length	9
Physical	SC
nTimeSamples	2680
codebook	2×2
PRI	0.5 ms
CPI	32
Total simulation time	1.34 sec

V. SIMULATION STUDY

The QD channel realization software in [16] allows a user to create scenarios with different environment settings. The inputs to the software include: three-dimensional (3D) environment geometry, target positions over time, node positions and rotations, and antenna positions and orientations. Via the geometric ray tracing technique, the software generates multipath components (MPCs) at each simulation step, specifying the values of path delay, gain, phase, AoA (angle of departure), AoD (angle of arrival) in both elevation and azimuth directions. In this paper, we present a human target as a point target, where the point target represents the human spine. One transmitter and seven receivers are placed in different locations of the room with their coordinates listed in Table I. The target is moving on a straight line with a moving speed of 1 m/s.

The ISAC-PLM software [17] uses the MATLAB Wlan-Toolbox with modifications to generate and process the IEEE 802.11bf signals. The QD output provides the necessary details on the communication channel, while the user can configure other system parameters. Table II lists some key parameters used in this work, where the physical layer adopts single carrier (SC) transmission, and the sampling frequency and the carrier frequency are denoted by f_s and f_c respectively. For a 2×2 antenna array, the codebook contains 25 antenna wave vector (AWVs) with 5 different azimuth and 5 different elevation angles [17]. The training length refers to the number of TRN units used in the BRP, and is chosen in order to cover the full codebook. We record the channel estimates at the receiver from the ISAC-PLM software to test our algorithms.

A. Measurement Accuracy at Individual Receivers

We first evaluate the accuracy of extracting the range estimate from each receiver using root mean square error (RMSE) over 20 Monte Carlo runs: $\text{RMSE}(z, \hat{z}) = \sqrt{\frac{1}{\text{MC}} \sum_{j=1}^{\text{MC}} (z_j - \hat{z}_j)^2}$, where z_j and \hat{z}_j represent the true range and the estimated range value in meters respectively, for the j th Monte Carlo run. A summary of the results for seven receivers at three different SNR levels are presented in Table III. Fig. 3 shows the scatter plots of the range estimates for each receiver at 20 dB. The estimates have high variations for receivers 1 and 5 whereas they linger around the same point for the remaining receivers. The estimates at receiver 3 has a large bias but with small variations. Receiver 7 was placed next to receiver 3 with 10 cm change in height. This minor

TABLE III
RMSE VALUES FOR DIFFERENT SNR LEVELS AND RECEIVERS.

SNR[dB]	Rx 1	Rx 2	Rx 3	Rx 4	Rx 5	Rx 6	Rx 7
20	3.741	0.143	1.562	0.119	1.017	0.044	0.163
30	0.041	0.143	1.562	0.052	0.222	0.044	0.163
50	0.041	0.143	1.562	0.027	0.222	0.044	0.136

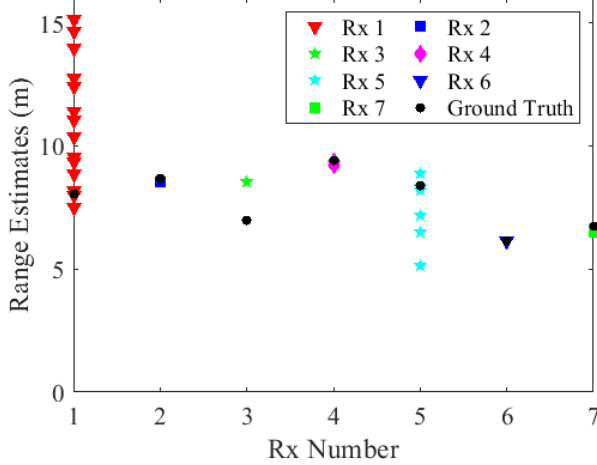


Fig. 3. Scatters of range estimates against the ground truth, SNR = 20 dB

change allowed the measurements at receiver 7 to increase the accuracy by 91% compared to receiver 3. This highlights the fact that *the range estimation accuracy is geometry dependent*.

The accuracy improves when the SNR increases from 20 dB to 30 dB. However, further increasing SNR to 50 dB does not help, which likely is due to the finite-grid search.

B. Localization Accuracy

The central receiver carries out the localization task, based on the range estimates at SNR of 30 dB. Two scenarios with different receiver selections are summarized in Table IV. If the estimates collected from all the receivers are used, the error values in Scenario B increases significantly with an error over one meter. Much smaller error is achieved in Scenario A using the range estimates of six out of seven receivers.

Fig. 4 shows the true track and the estimated track based on the receivers in Scenario A, with a zoomed picture of the track shown in in Fig. 5. One can see that the estimated track does go off the true track in certain points, however, the track is clearly retrieved, with errors as small as 0.7 cm and a maximum of 18 cm. The results in Table IV and Fig. 4 indicate that the target's track can be retrieved with good results, however, *the estimates from different receivers need to be censored*.

VI. CONCLUSION

In this paper, we presented a complete process of indoor localization with IEEE 802.bf signals in a multistatic setting with unsynchronized receivers. We identified the major signal processing tasks, and carried out a simulation study based on the QD channel simulator and the ISAC-PLM software package from NIST. The numerical study verifies the feasibility of

TABLE IV
MAXIMUM AND MINIMUM ERROR VALUES ALONG THE TRACK

	Rx Used	Max Error	Min Error
Scenario A	Rx 3 is excluded	0.1834 m	0.0078 m
Scenario B	All Rx's are used	1.3955 m	0.4701 m

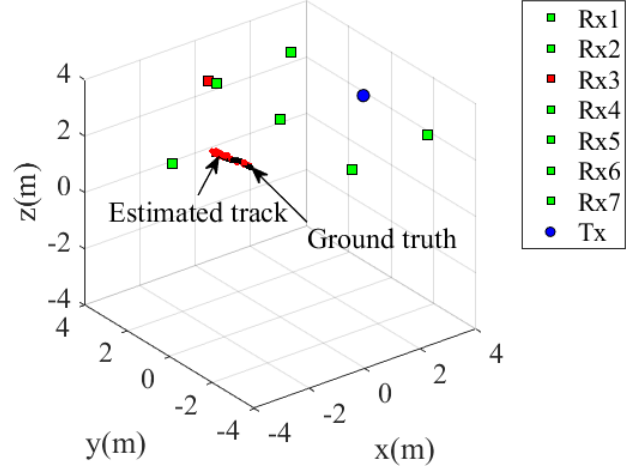


Fig. 4. The true track and the estimated track based on six out of seven receivers in Scenario A. The blue dot marks the location of the transmitter. The active receivers are shown in green squares and the inactive receiver is shown in a red square.

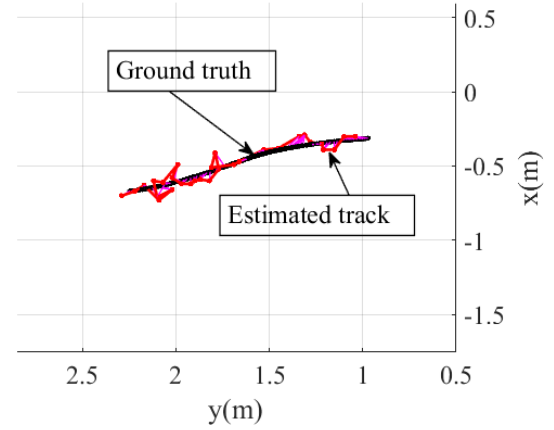


Fig. 5. The two-dimensional view of Fig. 4 that compares the estimated track against the ground truth.

accurate localization of the proposed approach and highlights the challenges. In particular, the range estimation accuracy is geometry dependent; hence, receiver placement and dynamic receiver selection will play significant roles in meeting the localization accuracy requirements.

Other future works will include: (1) study of an extended target (e.g., human) instead of a point target; (2) development of tracking algorithms that can manage to effectively fuse unreliable measurements from different receivers.

REFERENCES

- [1] Y. Ma, G. Zhou, and S. Wang, "WiFi Sensing with Channel State Information: A Survey," *ACM Comput. Surv.*, vol. 52, no. 3, June 2019. [Online]. Available: <https://doi.org/10.1145/3310194>
- [2] R. Du, H. Xie, M. Hu, Narengerile, Y. Xin, S. McCann, M. Montemurro, T. X. Han, and J. Xu, "An overview on IEEE 802.11bf: WLAN sensing," 2022.
- [3] C. Chen, H. Song, Q. Li, F. Meneghello, F. Restuccia, and C. Cordeiro, "Wi-Fi sensing based on IEEE 802.11bf," *IEEE Communications Magazine*, vol. 61, no. 1, pp. 121–127, 2023.
- [4] F. Meneghello, C. Chen, C. Cordeiro, and F. Restuccia, "Toward integrated sensing and communications in IEEE 802.11bf Wi-Fi networks," *IEEE Communications Magazine*, vol. 61, no. 7, pp. 128–133, 2023.
- [5] S. Blandino, T. Ropitault, C. R. C. M. da Silva, A. Sahoo, and N. Golmie, "IEEE 802.11bf DMG sensing: Enabling high-resolution mmWave Wi-Fi sensing," *IEEE Open Journal of Vehicular Technology*, vol. 4, pp. 342–355, 2023.
- [6] P. Kumari, N. Gonzalez-Prelcic, and R. W. Heath, "Investigating the IEEE 802.11ad standard for millimeter wave automotive radar," in *IEEE VTC2015-Fall*, 2015, pp. 1–5.
- [7] P. Kumari, J. Choi, N. González-Prelcic, and R. W. Heath, "IEEE 802.11ad-based radar: An approach to joint vehicular communication-radar system," *IEEE Transactions on Vehicular Technology*, vol. 67, no. 4, pp. 3012–3027, 2018.
- [8] G. Duggal, S. Vishwakarma, K. V. Mishra, and S. S. Ram, "Doppler-resilient 802.11ad-based ultrashort range automotive joint radar-communications system," *IEEE Transactions on Aerospace and Electronic Systems*, vol. 56, no. 5, pp. 4035–4048, 2020.
- [9] E. Grossi, M. Lops, L. Venturino, and A. Zappone, "Opportunistic radar in IEEE 802.11ad networks," *IEEE Transactions on Signal Processing*, vol. 66, no. 9, pp. 2441–2454, 2018.
- [10] E. Grossi, M. Lops, and L. Venturino, "Adaptive detection and localization exploiting the IEEE 802.11ad standard," *IEEE Transactions on Wireless Communications*, vol. 19, no. 7, pp. 4394–4407, 2020.
- [11] E. Grossi, M. Lops, A. M. Tulino, and L. Venturino, "Opportunistic sensing using mmwave communication signals: A subspace approach," *IEEE Transactions on Wireless Communications*, vol. 20, no. 7, pp. 4420–4434, 2021.
- [12] J. Wang, J. Chuang, S. Berweger, C. Gentile, and N. Golmie, "Towards opportunistic radar sensing using millimeter-wave Wi-Fi," *IEEE Internet of Things Journal*, pp. 1–1, 2023.
- [13] P. Wang and P. Boufounos, "Monostatic DMG passive sensing with hypothesis testing," in *Proc. of IEEE International Conference on Acoustics, Speech and Signal Processing (ICASSP)*, 2024, pp. 13 381–13 385.
- [14] J. Chuang, R. Caromi, J. Senic, S. Berweger, N. Varshney, J. Wang, C. Lai, A. Bodi, W. Sloane, C. Gentile, and N. Golmie, "Quasi-deterministic channel propagation model for human sensing: Gesture recognition use case," *IEEE Open Journal of Antennas and Propagation*, vol. 5, no. 3, pp. 557–572, 2024.
- [15] T. Kikuzuki, M. Boloursaz Mashhadi, Y. Ma, and R. Tafazolli, "Attention on the Preambles: Sensing With mmWave CSI," *IEEE Open Journal of the Communications Society*, vol. 5, pp. 6430–6442, 2024.
- [16] A. Bodi, S. Blandino, N. Varshney, J. Zhang, T. Ropitault, M. Lecci, P. Testolina, J. Wang, C. Lai, and C. Gentile, "NIST Quasi-Deterministic (Q-D) Channel Realization Software Documentation," March 2022. [Online]. Available: <https://www.nist.gov/services-resources/software/quasi-deterministic-channel-realization-software>
- [17] S. Blandino, T. Ropitault, N. Varshney, J. Wang, A. Sahoo, C. Gentile, and N. Golmie, "Integrated Sensing and Communication Physical Layer Model," 2022. [Online]. Available: <https://github.com/wigig-tools/isac-plm>